J. Membrane Biol. 214, 9–17 (2006)
DOI: 10.1007/s00232-006-0024-3

The Journal of
Membrane
Biology



# Electrokinetics of Miniature $K^+$ Channel: Open-State *V* Sensitivity and Inhibition by $K^+$ Driving Force

**Sabrina Gazzarrini[1], Alessandra Abenavoli[1], Dietrich Gradmann[2], Gerhard Thiel[3], Anna Moroni[1]**
[1]Department of Biology and IBF-CNR, Università degli Studi di Milano, Via Celoria 26, 20133 Milan, Italy
[2]A.-v.-Haller-Institut der Universität, Untere Karspüle 2, 37073 Göttingen, Germany
[3]Botanisches Institut, Technischen Universität, Schnittspahnstr. 3, 64287 Darmstadt, Germany

Received: 23 April 2006/Revised: 26 October 2006

**Abstract.** Kcv, isolated from a *Chlorella* virus, is the smallest known $K^+$ channel. When Kcv is expressed in *Xenopus* oocytes and exposed to 50 mM $[K^+]_o$, its open-state current-voltage relationship (*I-V*) has the shape of a "tilted S" between −200 and +120 m*V*. Details of this shape depend on the conditioning voltage ($V_c$) immediately before an *I-V* recording. Unexpectedly, the *I-V* relationships, recorded in different $[K^+]_o$, do intersect. These characteristics are numerically described here by fits of a kinetic model to the experimental data. In this model, the $V_c$ sensitivity of *I-V* is mainly assigned to an affinity increase of external $K^+$ association at more positive voltages. The general, tilted-S shape as well as the unexpected intersections of the *I-V* relationships are kinetically described by a decrease of the cord conductance by the electrochemical driving force for $K^+$ in either direction, like in fast *V*-dependent blocking by competing ions.

**Key words:** Electrophysiology — Enzyme kinetics — $K^+$ channel — Open state — Selectivity filter — *Xenopus* expression

## Introduction

The $K^+$ channel Kcv from a *Chlorella* virus (Plugge et al., 2000) is the smallest known $K^+$ channel with only 94 amino acids. Corresponding to the known crystal structure of a similar bacterial channel (Doyle et al., 1998), the monomers of Kcv consist of two membrane-spanning domains and a lumenal loop between the two membrane-spanning domains with the signature sequence of the $K^+$ selectivity filter. In Kcv, the cytoplasmic domains of the C and N termini are virtually absent. The functional unit is assumed to be a homotetramer. Because of the extremely reduced cytoplasmic termini, Kcv is understood to represent an extremely simple and possibly primordial $K^+$ channel without regulating sites, which are usually found in the cytoplasmic termini. Therefore, the electrical properties of Kcv are of fundamental interest as a model system for the transport function of related but more complex channels.

Initial voltage-clamp studies of the electrical properties of Kcv showed a voltage-sensitive steady-state conductance and two exponential components of the tail-current relaxations (Gazzarrini et al., 2002) in the resolved time range >1 ms. These properties can be described by a gating scheme O1-O2-C with two open states, O1 and O2, of the same conductance ($G_1 = G_2$) and a closed state, C. This gating model comprises a *V*-independent equilibrium, $P_{O2}$:$P_C \approx$ two-thirds of the occupancies between states O2 and C at positive *V*, whereas at negative *V*, the conductance reaches maximum $P_{O1} = 1$, with a characteristic voltage of about −80 m*V*, where $P_{O1} = P_{O2}$. Kcv gating, however, is no major subject here. We rather focus on the apparent open state characteristics of this channel, including possible gating functions which are much faster than the temporal resolution of the recording system of about 1 ms.

The simplifying assumption $G_1 = G_2$ seems to be supported by the similar shape of the steady-state *I-V* relationship, no matter whether it is recorded after negative (favoring O1) or after positive (favoring O2) conditioning voltages ($V_c$) (Gazzarrini et al., 2002).

The characteristic shape of the Kcv open channel *I-V* relationship consists of a current decrease at large *V* deviations of either sign from equilibrium, resulting in a pronounced current maximum in the positive *V*

*Correspondence to:* D. Gradmann; email: dgradma@uni-goettingen.de

range and a corresponding minimum in the negative one (Plugge et al., 2000; Gazzarrini et al., 2002). This "tilted-S" shape does not follow the common Goldman-Hodgkin-Katz model for electrodiffusion (linear *I-V* at $|V| >> 0$), the familiar model of a series of Eyring barriers (exponential rising *I-V* at $|V| >> 0$) or conventional Michaelis-Menten kinetics (constant *I* at $|V| >> 0$).

A general effect of diffusion limitation can be ruled out as well since recent studies of Kcv expressed in HEK cells showed that the characteristic tilted-S shape of the open channel *I-V* can be specifically assigned to wild-type (wt) Kcv, whereas the open channel *I-V* relationships of mutated Kcv are much more linear (Hertel et al., 2006).

However, this characteristic tilted-S shape seems to correspond to the changes of the shape of *I-V* relationships due to fast *V*-dependent block by competing cations (Klieber & Gradmann, 1993). Especially $Mg^{2+}$ has to be discussed in this context (Nichols & Lopatin 1987). However, since changes of $[Mg^{2+}]_o$ do not cause a corresponding change of the current minimum in the *I-V* of Kcv (Gazzarrini et al., 2002), fast *V*-dependent block by $Mg^{2+}$ should be ruled out as the main mechanism for the tilted-S shape of this *I-V*. Nevertheless, the concentrations of possibly competing ions of this $K^+$ channel are kept small in this study in order to virtually exclude their inhibiting influence.

Correspondingly, the internal concentrations of possibly competing cations are considered to be small compared to $[K^+]_i$.

Alternatively, we suggest here that large driving forces of $K^+$ itself inhibit the $K^+$ conductance of wt-Kcv in an equivalent, fast and *V*-dependent mode.

A kinetic understanding of these channel characteristics of wt-Kcv is the general aim of this study. The underlying concept consists of a kinetic analysis of nonlinear *I-V* relationships (Gradmann & Boyd 2004, 2005).

This concept is applied here to specific problems. One of the problems investigated is the question of whether the states O1 and O2 differ, in fact, only by their *V*-dependent occupancy ($P_{O1} > P_{O2}$ at $V << 0$ and *vice versa*) and not by their kinetic characteristics. This mode would only amount to a simple $V_c$-dependent current scaling of the *I-V* relationship without change in shape. Alternatively, the two states may have the same *V*-independent occupancies but different kinetics ($G_1 > G_2$ at $V << 0$ and *vice versa*). Combinations of the two scenarios can be thought of as well, of course. Here, we present evidence for the second scenario.

The second specific problem addresses the following well-known situation. Suppose there are two steady-state *I-V* relationships of a charge-translocating enzyme, which are recorded under two different substrate concentrations at one of the two

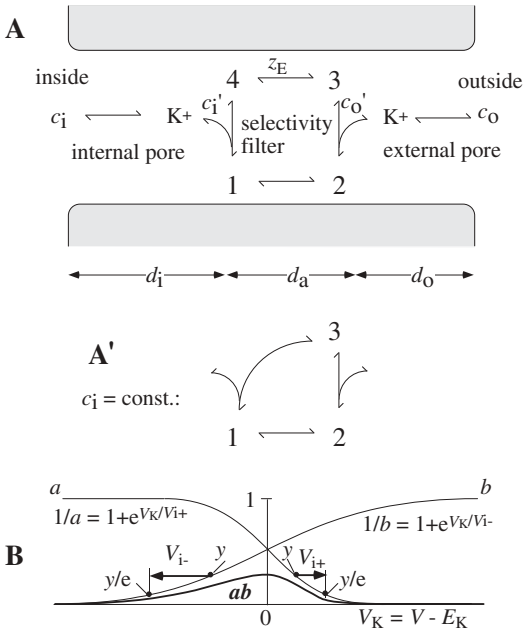


**Fig. 1.** Working hypothesis with definitions for formal treatment. (*A*) General reaction scheme for an active ion translocating enzymes according to Gradmann & Boyd (2005). (*A'*) Simplified three-state version of *A* under assumption of constant $c_i$ (internal concentration) and variable $c_o$ (external concentration) during experimentation. (*B*) Formalism for inhibition of cord conductance $G_c$ from its maximum at zero driving force for $K^+$, $V_K = V - E_K$, toward zero by $|V_K| > 0$ with inhibition coefficients $V_{i+}$ and $V_{i-}$ for positive and negative voltages, respectively; the product of two asymmetric Boltzmann functions, *a* and *b*, with opposite slopes assumes the bold (asymmetric) bell shape of the activity/voltage relationship.

sides of the membrane. For thermodynamic reasons (Fingerle & Gradmann, 1982; Blatt, 1986), these two *I-V* relationships will not intersect under ordinary circumstances. If such intersections are nonetheless observed, it means that the substrate has not only a normal stoichiometric role in the kinetics but also an additional allosteric effect. Such noncanonical intersections do occur in the *I-V* relationships of Kcv. The corresponding kinetics are analyzed here by a version of the standard kinetic model (Gradmann & Boyd 2004) in which transport activity is inhibited by electrochemical $K^+$ driving forces ($V_K = V - E_K$) of either sign. This formalism is able to describe the bell-shaped $G_c(V_K)$ relationship of the cord conductance with a maximum $G_c$ at $V_K = 0$, which is deduced from the experimental data here.

Recently, it has been shown that the tilted-S shape of *I-V* will arise when the apparent charge number, $z_E$ (Fig. 1A), of the empty binding site of the ion-translocating enzyme and the apparent charge number, $z_C = z_E + z_{K+}$, of the complex have the same sign (Gradmann & Boyd, 2005). Although the data presented here point to this mechanism in Kcv,

they also call for an additional mechanism to explain the intersecting *I-V* relationships when the substrate concentration has changed on one side of the membrane.

## Materials and Methods

### TECHNICAL

Electrophysiological experiments with Kcv from the large *Chlorella* virus PBCV-1 (Plugge et al., 2000) heterologously expressed *Xenopus* oocyte were technically performed as described before (Gazzarrini et al., 2002). Briefly, Kcv cDNA was cloned into pSGEM vector (a modified version of pGEM-HE; courtesy of M. Hollmann, Max Planck Institute for Experimental Medicine, Göttingen, Germany). cRNA was transcribed *in vitro* using T7 RNA polymerase (Promega, Madison, WI) and injected (50 ng/oocyte) into *Xenopus laevis* oocytes, prepared according to standard methods. Measurements were performed 2–4 days after injection.

Currents were recorded using a two-electrode voltage-clamp amplifier (Geneclamp 500; Axon Instruments, Foster City, CA) under control of pCLAMP8 software (Axon Instruments). Electrodes were filled with 3 M KCl and had a resistance of 0.4–0.8 MΩ in 50 mM KCl. The oocytes were perfused at room temperature with a standard bath solution containing 50 (or 20 or 100) mM KCl, 1.8 mM $CaCl_2$, 1 mM $MgCl_2$ and 5 mM 4-(2-hydroxyethyl)-1-piperazineethanesulfonic acid (HEPES)/KOH (pH 7.4) at a rate of 2 ml $\cdot$ $min^{-1}$. Mannitol was used to adjust the osmolarity of the solution to 215 mOsmol/liter.

### THEORETICAL

The model used here and definitions of its system parameters are shown in Figure 1. Figure 1A illustrates a general model for the kinetic description of the transport function of an ion transporter according to Gradmann & Boyd (2004, 2005). Basically, it consists of an enzymatic four-state cycle, which senses the fraction $d_a$ of the transmembrane voltage. It operates as the active center between an inner and an outer access section of free electrodiffusion, which sense the corresponding fractions $d_i$ and $d_o$ of $V$. The empty binding site of the enzyme carries the apparent charge $z_E$.

For the present study, only three states of the enzymatic transport cycle were assessed because the internal substrate concentration had to be assumed to change nonsignificantly during the experimental procedure. The correspondingly simplified part of the reaction scheme is given by Figure 1A′. Thus, the equation of the steady-state current-voltage relationship through $n$ active transporter molecules in the membrane is as follows:

$$I = n\, z_{K^+}\, e \frac{k_{31}k_{12} - K_2 k_{21}k_{13}}{K_2(k_{12}+k_{21}+k_{13})+k_{12}+k_{13}+k_{31}} f_i \qquad (1)$$

with the elementary charge $e = 1.6\ 10^{-19}$As, the rate constants

$$k_{12} = k_{12}{}^0 \exp(d_a z_C u/2) \qquad (2a)$$

$$k_{21} = k_{21}{}^0 \exp(-d_a z_C u/2) \qquad (2b)$$

$$k_{13} = k_{13}{}^0 \exp(d_a z_E u/2) \qquad (2c)$$

$$k_{31} = k_{31}{}^0 \exp(-d_a z_E u/2) \qquad (2d)$$

where the superscript zero marks the $k_{ij}$ values at $V = 0$, $z_C = z_E + z_{K+}$ is the apparent charge number of the occupied binding site, $u = VF/(RT)$ is the reduced transmembrane voltage and the factor 1/2 in the exponent stands for the assumption of symmetric Eyring barriers. The stability constant for state 2, $K_2 = k_{32}/k_{23}$, reflects the assumption of large rate constants for binding ($k_{32} = k_{32}{}^0 c_o'$, with $k_{32}{}^0 = k_{32}$ at $c_o' = 1$ mM immediately at the outward oriented binding site) and debinding ($k_{23}$) compared with small $k_{12}$, $k_{21}$, $k_{13}$ and $k_{31}$ which comprise conformational changes. Microscopic reversibility dictates $K_2{}^0 = k_{31}{}^0 k_{12}{}^0/(k_{21}{}^0 k_{13}{}^0) = K_2$ at 1 mM $c_o'$ and $V = 0$. The fast equilibrium reactions $k_{23}$ and $k_{32}$ themselves are assumed to be $V$-insensitive, whereas $V$ enters $K_2$ via

$$c_o' = c_o \exp(-d_o z_{K+} u) \qquad (3)$$

in $K_2 = K_2{}^0 c_o'$. Corresponding relationships hold for $K_1$ in the explicit model of Figure 1A. In the simplified version of Figure 1A′, the internal access section $d_i$ enters the system by a corresponding $c_i' = c_i \exp(d_i z_{K+} u)$ and $k_{13} = k_{13}{}^0/c_i'$[1].

The inhibiting factor

$$f_i = 1/[1+\exp(V_K/V_{i+})]/[1+\exp(V_K/V_{i-})] \qquad (4)$$

in equation 1 reflects the effect of the driving force, $V_K = V - E_K$, ($E_K$ is the Nernst equilibrium voltage for electrodiffusion of $K^+$) on the transport function, where the inhibition coefficients $V_{i+}$ and $V_{i-}$ mark $V$ spans for an $e$-fold current reduction in the respective branch of the bell-shaped $f_i(V_K)$ curve. Figure 1B illustrates the $V$ dependence of $f_i$.

The custom-tailored software for numerical analysis of the experimental data is written in Turbo-Pascal and available on request.

## Results

### BASIC OBSERVATION

Instantaneous *I-V* relationships were recorded by *V*-clamp, applying $V$ steps of various sizes starting from a conditioning voltage $V_c$ (Fig. 2). The current values were taken about 2 ms after the change in command voltage, when the recorded $V$ had reached a steady state and the partly compensated capacitative current transient had essentially vanished. Only at very positive voltages in Figure 2D, were the currents not settled completely. The resulting inaccuracy does not affect our qualitative conclusions. No sig-

[1] The relationship between the rate constants $k_{34}$, $k_{43}$, $k_{14}$, $k_{41}$ in the detailed model Fig. 1A and the gross rate constants $k_{13}$ and $k_{31}$ in the reduced model of Fig. 1A′ is

$$k_{31} = k_{34}\, k_{41}/(k_{41}+k_{43}) \qquad (5a)$$

$$k_{13} = k_{14}\, k_{43}/(k_{41}+k_{43}). \qquad (5b)$$

With the assumption $k_{34}, k_{43} << k_{14}, k_{41}$, Eqs. 5a,b degenerate to a) $k_{31} = k_{34}\ k_{41}/k_{41} = k_{43}$ and b) $k_{13} = k_{14}\ k_{43}/k_{41} = k_{14}k_{43}/(k_{41}{}^0 c_i') = k_{13}{}^0/c_i'$, where $k_{41}{}^0$ is $k_{41}$ at reference conditions ($c_i' = 1$ mM). This means $c_i$ enters the system actually by the denominator of $k_{13}$ and not by the numerator of $k_{31}$ as might intuitively be assumed for a ligand.

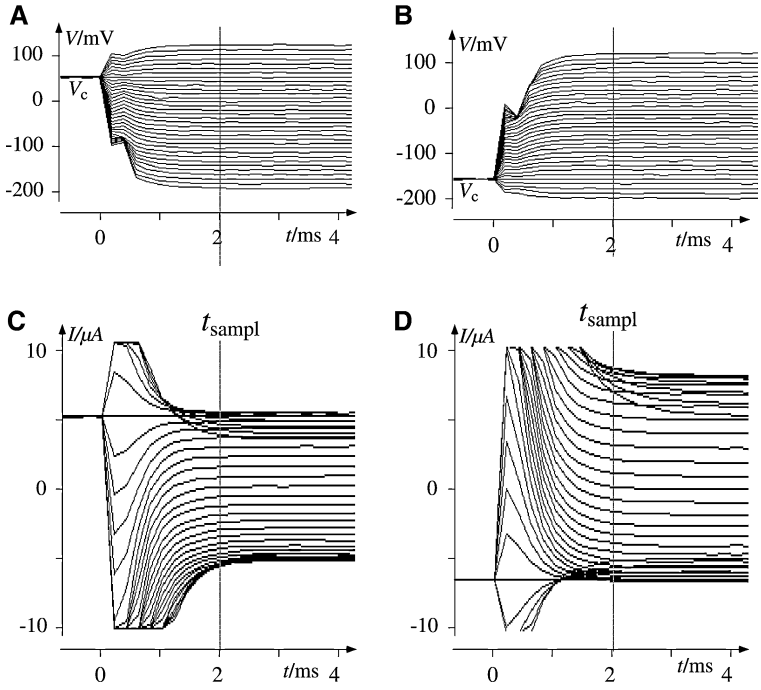


**Fig. 2.** Original records of $V(t)$ and $I(t)$ in voltage-clamp experiments of *Xenopus* oocytes with heterologously expressed Kcv. (*A, C*) Recorded voltages and currents upon stepwise changes of the command voltage from a conditioning voltage $V_c = +60$ m$V$ to a new $V$ level, approximately equally spaced in 10-m$V$ intervals from −200 to +120 m$V$. Instantaneous $I$-$V$ points taken at about 2 ms ($t_{sample}$) after change command voltage, when recorded voltage had reached an approximate steady state and capacitive current transient (partly compensated) was essentially over. (*B, D*) Same as *A* and *C* but with a conditioning voltage $V_c = -160$ m$V$.

nificant differences of these instantaneous $I$-$V$ relationships could be found whether the $V$ steps have been applied in ascending or descending order (*data not shown*), which means that these instantaneous currents were not biased by nonresolved temporal components.

In the $V$-clamp experiments, the $V$ steps of the command voltage were equally spaced in 10-mV intervals. After optimizing the temporal resolution of the recording system by gain and capacity compensation of the amplifier, the measured voltage did not match the command voltage exactly. In these cases, we fitted a seventh-order polynomial function to the experimental $I$-$V$ curve (example in Fig. 3) and calculated the currents for the applied, equally spaced command voltages by interpolation. Since these corrected $I$-$V$ relationships did not differ from the recorded ones by more than 1%, the more convenient, corrected $I$-$V$ records with equally spaced voltages were used for further analysis. Figure 3 shows also the accuracy and reproducibility of the experimental $I$-$V$ recordings in this study, given by the normalized means ± standard deviation of the equally spaced (10 mV) $I$-$V$ relationships after polynomial fitting.

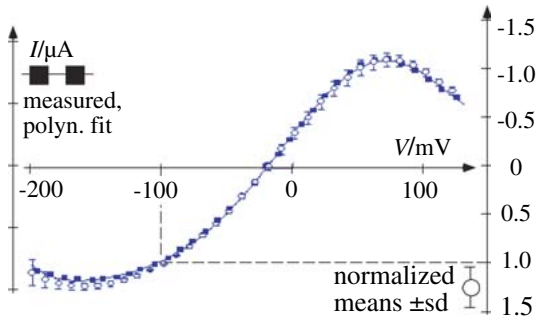


**Fig. 3.** Reproducibility of experimental results. *Solid squares*, originally recorded $I$-$V$ relationship with not quite equally spaced 10-m$V$ intervals (due to imperfect $V$ clamp). *Curve through solid squares*, fit of seventh-order polynomial to experimental data, allowing reconstruction of $I$-$V$ relationship with perfect 10-m$V$ spacing for further processing. *Open circles with error bars*, means ± standard deviation of $n = 13$ $I$-$V$ curves in equally spaced 10-m$V$ intervals from polynomial fits, normalized to $I$ at −100 m$V$ (−5.99 ± 0.05 μA).

## The Problem of $V$ Gating in Kcv

A fundamental task in understanding channel kinetics is recognition of a valid $V$-gating scheme, i.e., the assignment of the experimental data to a reaction system with various conducting (and nonconducting) states and the respective, voltage-dependent transition probabilities between these states.

Within the accuracy of previous recordings (Gazzarrini et al., 2002), the effect of $V_c$ on the macroscopic $I$-$V$, like in Figure 4A, was interpreted as a matter of familiar $V$ gating, meaning that the time-averaged number of open channels (open probability, $P_O$) changes with $V_c$, whereas the apparent single-channel open state $I$-$V$ relationship is basically constant.

Here, series of $I$-$V$ relationships were recorded with alternating $V_c$ of −160 or +60 m$V$. From many experiments, only those seven records were accepted which showed best coincidence between pre- and postcontrol records; i.e., an $I$-$V$ relationship with

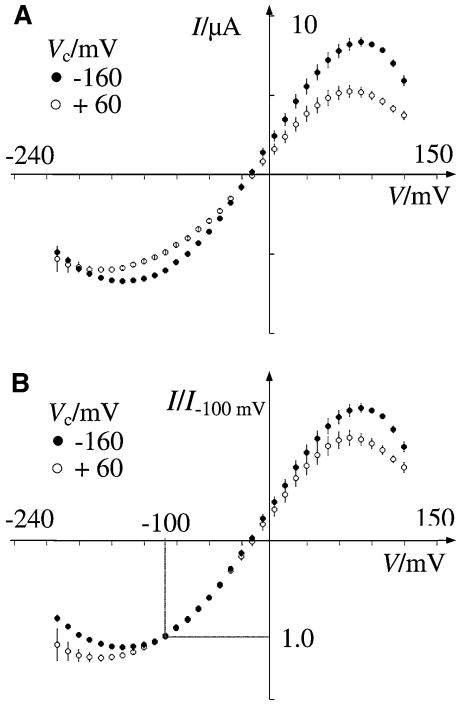


**Fig. 4.** Impact of conditioning voltage $V_c$ on open state *I-V* curve of Kcv. (*A*) Mean results ($n = 7$ oocytes) from $V_c = -160$ m*V* and $V_c = +60$ m*V*; mean current from $V_c = +60$ m*V* at $-100$ m*V* was (81 ± 2 standard error)% of the control current from $V_c = -160$ m*V*. (*B*) Same data as in *A* but normalized to the current at $-100$ m*V*, indicating no simple scaling effect of $V_c$ as expected for gating but significant change of *I-V* shape.

$V_c = +60$ m*V* was only accepted for those seven records which showed the best coincidence of the $V_c = -160$ m*V* records before and after the $V_c = +60$ m*V* measurement in between.

These records (Fig. 4) show that the effect of $V_c$ on *I-V* does not consist of a simple scaling. The difference in curvatures of the two *I-V* relationships from $V_c = -160$ m*V* and $V_c = +60$ m*V* becomes evident when the curves are normalized to the same macroscopic current at $-100$ m*V* (Fig. 4B). The corresponding scaling factor of 0.81, which was previously assigned to a *V*-dependent change in $P_O$ only (Gazzarrini et al., 2002), must be discussed now as a matter of *V* sensitivity of apparent single-channel kinetics as well. The answer is provided by the numerical analysis below.

## Fits

Fitting the model to the data should provide not only a good mathematical description of the experimental data but also criteria for the physical validity of the approach. For the former purpose, the fits usually improve with the number of free parameters. In contrast, the latter purpose demands a minimum of free parameters for a unique solution. The strategy applied here focuses on a skeleton model with the aim of identifying the major processes which determine the electrical behavior of the channel. The final fits are, therefore, not the best ones because minor effects are ignored. On the other hand, these numerically somewhat inferior fits with a minimum of free parameters yield the desired nonambiguity of the solutions. The explicit strategy comprised several *ad hoc* decisions depending on the respective numerical results, as documented in Table 1.

All fits were applied to quadruplets of experimental *I-V* relationships, differing in $[K^+]_o$ and $V_c$. The first step was to estimate the number ($n \approx$ 500,000) of active channels expressed in the oocyte membrane. This was done by dividing the maximum slope conductance ($G_s \approx 60$ μS) of the *I-V* curve in 50 mM $[K^+]_o$ from $-160$ m*V* $V_c$ by the 120-pS single-channel conductance of Kcv (Pagliuca et al. 2007). Very good fits (errors around 300 nA) could be obtained when all fitted parameters, $z_E$ to $V_{i+}$ (except $[K^+]_i$), were allowed to differ between the two $V_c$ conditions. However, since many combinations of the 19 free parameters resulted in equally good fits (*not shown*) depending on the start parameters, these results were physically meaningless. Therefore, we assumed $z_E$, $d_i$, $d_o$, $[K^+]_i$, $V_{i+}$ and $V_{i-}$ to be $V_c$ - insensitive and obtained good fits with the reduced number of 10 independent parameters (Table 1, A).

Interestingly, $d_i$ and $d_o$ turned out to be quite small in these fits. Consequently, fits with fixed $d_i$, $d_o = 0$ were essentially equally good (Table 1, B). These fits with the reduced number of eight free parameters show, depending on the start parameters, a small variability of $z_E$, ${k_{12}}^0$, $[K^+]_i$, $V_{i+}$ and $V_{i-}$ and considerable variability of the fundamental rate constants ${k_{21}}^0$, ${k_{13}}^0$ and ${k_{31}}^0$. In particular, ${k_{21}}^0$ either converged to values around $10^{10} \cdot s^{-1}$ or diverged to unrealistic $> 10^{14} \cdot s^{-1}$ (realistic is $\leq 10^{11} \cdot s^{-1}$). These observations are documented in Table 1 (A–I).

In order to identify the kinetic impact of $V_c$ in the model in Figure 1, we started with the simplest hypothesis, namely that this effect can mainly be assigned to the change in a single parameter of the model. For this purpose, we kept every parameter for the two $V_c$ conditions in common, except the one of the individual candidate under scrutiny, which was allowed to differ between $V_c = -160$ m*V* and $V_c = +60$ m*V*. The results of this test of each candidate are listed in Table 1 (C–I). Judged by the magnitudes of the error, only multiplication of ${k_{13}}^0$ (Table 1, F) or division of ${k_{31}}^0$ (Table 1, G) by approximately 2 can explain the difference of *I-V* between $V_c = -160$ m*V* and $V_c = +60$ m*V* by a change of a single parameter. We are inclined to reject the ${k_{13}}^0$ solution (Table 1, F) because the numerical results of ${k_{13}}^0 > 10^{14} \cdot s^{-1}$ is unrealistically high and because the fit of the ${k_{31}}^0$ solution (Table 1, G) is better. This accepted solution, however, yields a

**Table 1.** Numerical results of fitting model in Figure 1 to experimental data as shown in Figure 5

| | Conditions | | Results | | | | | | | | | | | |
|---|---|---|---|---|---|---|---|---|---|---|---|---|---|---|
| | $[K^+]_o$ (mM) | $V_c$ (mV) | $z_E$ | $d_i$ (%) | $d_o$ (%) | $k_{12}^0$ ($M \cdot s^{-1}$) | $k_{21}^0$ ($G \cdot mM \cdot s^{-1}$) | $k_{13}^0$ ($G \cdot mM \cdot s^{-1}$) | $k_{31}^0$ ($G \cdot mM \cdot s^{-1}$) | $[K^+]_i$ (mM) | $V_{i+}$ (mV) | $V_{i-}$ (mV) | Err (nA) |
| A | 50/20 | Start | 0 | 10 | 10 | 100 | 10 | 10 | 1 | 100 | 100 | −100 | 346 |
| | | −160 | 0.66 | 3.3 | 0.3 | 523 | 5.7 | 2,283 | 294 | 110 | 40 | −127 | |
| | | +60 | ″ | ″ | ″ | 435 | 2.0 | 5,534 | 462 | ″ | ″ | ″ | |
| B | | Start | 0 | 0 | 0 | 100 | 10 | 10 | 1 | 100 | 100 | −100 | 343 |
| | | −160 | 0.66 | ″ | ″ | 524 | 6.1 | 2,309 | 277 | 110 | 41 | −127 | |
| | | +60 | ″ | ″ | ″ | 434 | 2.1 | 5,143 | 415 | ″ | ″ | ″ | |
| C | | Start | 1 | 0 | 0 | 500 | 6 | 10 | 10 | 100 | 50 | −120 | 935 |
| | | −160 | 0.65 | ″ | ″ | 582 | 19,609 | 5,028 | 82 | 108 | 59 | −112 | |
| | | +60 | 0.71 | ″ | ″ | ″ | ″ | ″ | ″ | ″ | ″ | ″ | |
| D | | −160 | 0.68 | ″ | ″ | 545 | 8,438 | 1,729 | 66 | 105 | 59 | −169 | 612 |
| | | +60 | ″ | ″ | ″ | 402 | ″ | ″ | ″ | ″ | ″ | ″ | |
| E | | −160 | 0.64 | ″ | ″ | 503 | 30.1 | 4,338 | 247 | 110 | 44 | −114 | 469 |
| | | +60 | ″ | ″ | ″ | ″ | 1.06 | ″ | ″ | ″ | ″ | ″ | |
| F | | −160 | 0.64 | ″ | ″ | 566 | 2,712 | 10,717 | 271 | 110 | 59 | −95 | 429 |
| | | +60 | ″ | ″ | ″ | ″ | ″ | 19,572 | ″ | ″ | ″ | ″ | |
| G | | −160 | 0.65 | ″ | ″ | 540 | 15,855 | 4,087 | 1,225 | 109 | 52 | −114 | 417 |
| | | +60 | ″ | ″ | ″ | ″ | ″ | ″ | 676 | ″ | ″ | ″ | |
| H | | −160 | 0.69 | ″ | ″ | 487 | 4.4 | 2,851 | 442 | 112 | 42 | −155 | 505 |
| | | +60 | ″ | ″ | ″ | ″ | ″ | ″ | ″ | ″ | 35 | ″ | |
| I | | −160 | 0.73 | ″ | ″ | 446 | 16.2 | 954 | 77 | 107 | 49 | −393 | 915 |
| | | +60 | ″ | ″ | ″ | ″ | ″ | ″ | ″ | ″ | ″ | −5.E4 | |
| J | | −160 | 0.68 | ″ | ″ | ″ | ″ | 4,433 | 203 | ″ | ″ | ″ | 449 |
| | | +160 | ″ | ″ | ″ | ″ | ″ | ″ | 103 | ″ | ″ | ″ | |
| K | 50/100 | Start | 1 | 0 | 0 | 400 | 5.0 | 10 | 10 | 125 | 60 | −90 | 1,520 |
| | | −160 | 0.60 | ″ | ″ | ″ | ″ | 6,732 | 80 | ″ | ″ | ″ | |
| | | +60 | ″ | ″ | ″ | ″ | ″ | ″ | 39 | ″ | ″ | ″ | |
| L | Round. | −160 | 0.6 | 0 | 0 | 500 | 5 | 5,000 | 100 | 100 | 50 | −100 | |
| | | +60 | ″ | ″ | ″ | ″ | ″ | ″ | 50 | ″ | ″ | ″ | |

All data calculated for $n = 500{,}000$ channels in oocyte membrane, as determined by $n = G/\gamma$ with maximum slope conductance $G$ of oocyte membrane and single-channel conductance $\gamma = 120$ pS. Error data between lines for $V_c = -160$ and $V_c = +60$ m$V$ mark simultaneous fits to both sets of experimental $I$-$V$ data. Note, " in $V_c = -160$ lines means that the respective parameter value was fixed at the given start value; " in $V_c = +60$ lines means that the respective parameter value was forced to be the same for $V_c = +60$ m$V$ and for $V_c = -160$ m$V$.

very high (diverging?) value of $k_{21}^0$. This flaw could be circumvented by fixing $k_{21}^0$ at 6 x $10^9 \cdot s^{-1}$, which turned out to yield equally good fits (Table 1, J). When $k_{21}^0$ and the low variance parameters $k_{12}^0$, $[K^+]_i$, $V_{i+}$ and $V_{i-}$ are fixed at likely and rounded start values, the fits converge always to the same values of $z_E$, $k_{13}^0$, $k_{31}^0{}_{-160mV}$ and $k_{31}^0{}_{+60mV}$ (Table 1, J; Fig. 5A, B), independent of the start parameters within the limits of an order of magnitude (*data not shown*). Application of the same strategy to the results from the experiments with 50/100 mM $[K^+]_o$ yields similar results (Table 1, K; Fig. 5C, D). Thus, a global approximation with rounded parameters can be given (Table 1, L). The high value of $k_{13}^0 \approx 10^{12} \cdot s^{-1}$ in these results (Table 1, J–L) is not unrealistic. This value refers to a fundamental rate constant at 1 mM $[K^+]_i$ and has to be divided by $[K^+]_i \approx 100$ mM to obtain the realistic apparent rate constant $k_{13}$ in the range of $10^{10} \cdot s^{-1}$.

In conclusion, the effect of $V_c$ on $I$-$V$ cannot be assigned to ordinary $V$ gating, i.e., $V$-dependent change of the number of active channels and corresponding up-/downscaling of the macroscopic $I$-$V$ relationship without change in shape. Our results rather indicate that the number of active channels is independent of $V_c$, whereas the observed $V_c$-induced difference can mainly be assigned to a change in $k_{31}^0$ only. This solution includes a concomitant change of the equilibrium $K_2 = k_{32}/k_{23}$ due to $K_2^0 = k_{31}^0 k_{12}^0/(k_{21}^0 k_{13}^0)$, i.e., a change of $pK = -\lg(K_2^0/M)$ from

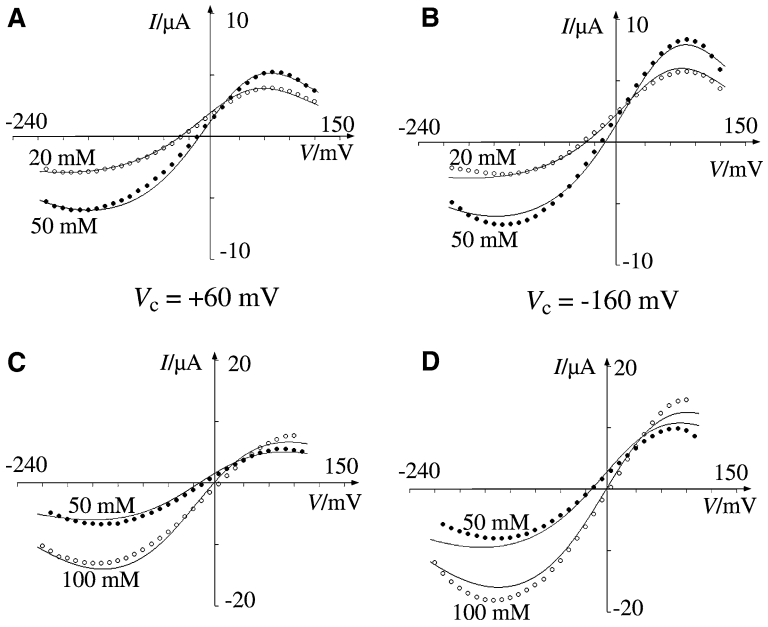


**Fig. 5.** Fits of model in Figure 1 to quadruplets of *I-V* curves, differing in $V_c$ and $[K^+]_o$ conditions as marked; mean experimental data. For statistical aspects, see Figure 3. Numerical results of fit to experimental data A and B (50/20 mM $[K^+]_o$) in Table 1 (J) to data C and D (50/100 mM $[K^+]_o$) in Table 1 (K). Note, these are not the best but unambiguous fits. Families of better descriptions were obtained (e.g., Table 1, A and B) by fits with more variable parameters.

$pK \approx -0.3$ at $-160$ m$V$ to $pK \approx 0.0$ at $+60$ m$V$ or an increase of the external affinity from half-saturation at $\approx 3$ M at $-160$ m$V$ to $\approx 1$ M at $+60$ m$V$. The good fits in Figure 5 mean also that the inhibition function $f_i$ of equation 4 is suitable to account for an intersection of *I-V* relationships from different $[K^+]_o$, as observed in Kcv.

## Discussion

Before discussing the results in detail, we point out that the tilted-S shape of the instananeous *I-V* relationship of wt-Kcv is not a matter of the particular expression system (*Xenopus* oocytes) used here. The shape is also observed when wt-Kcv is expressed in HEK cells (Hertel et al., 2006). Thus, the results presented here are likely to be genuine properties of the channel and not biased by peculiarities of the expression system.

Because of the model character of Kcv for the pore module of $K^+$ channels in general, the electroenzymatic impact of the individual model parameters is of general interest. The quality and stability of the fits in Figure 5 mean that the model in Figure 1 with $d_i$, $d_o = 0$ is appropriate to describe the experimental data. This means that the open channel conductance is limited by the selectivity filter and not by a possible bundle crossing of the monomers at the cytoplasmic mouth. If the latter were the case, a significant $d_i > 0$ would have been expected.

### Impact of Individual Parameters

Figure 6 shows the effect of a change (mostly doubling) of each parameter on the shape of a reference *I-V* relationship. This reference curve (fits and data) is replotted from Figure 5A (50 mM) in Figure 6A. All the other panels of Figure 6 show this reference curve as a thin line, and the particular changes are illustrated as bold lines in comparison.

Compared with the reference curve, doubling of the apparent charge $z_E$ of the empty binding site from 0.68 to 1.36 (Fig. 6B) causes the transport function with $z_E/z_C > 0$ to approach zero current much faster (more curvature) with large voltages of either sign.

Although the results in Table 1 (A) point to negligible electrical distances $d_i$ and $d_o$, i.e., to exposure of the active enzymatic reaction cycle to the full transmembrane voltage ($d_a \approx 1$), Figure 6C and D shows the theoretical impact of substantial distances $d_i$ and $d_o$ on *I-V* of Kcv. This impact results mainly in less curvature of *I-V* due to a reduced $V$ sensitivity of the rate constants (equation 1) by a smaller $d_a$. Due to the particular $z_E = 0.68$ (and $z_C = 1.68$), the increases of $d_i$ and $d_o$ from 0 to 0.1 have more effect in the negative $V$ range than in the positive one, gradually in case of $d_i$ and exclusively in case of $d_o$.

The effect of doubling $k_{12}$ (Fig. 6E) is very strong and essentially consists of a proportional upscaling. This is the reason for the high reproducibility of the $k_{12}{}^0$ values throughout the fits (Table 1, A–J). In contrast, the corresponding impact of $k_{21}{}^0$ is very weak and can only be visualized by a very large change (factor 50 in Fig. 6F).

Figure 6G and H shows the complementary effects of doubling $k_{13}$ and $k_{31}$, respectively, mainly in the positive $V$ range: doubling of $k_{13}$ causes stronger curvature and thus a smaller current peak, located at a less positive $V$ than in the reference *I-V*. Correspondingly, upon doubling of $k_{31}$, this peak is higher and located at more positive $V$.

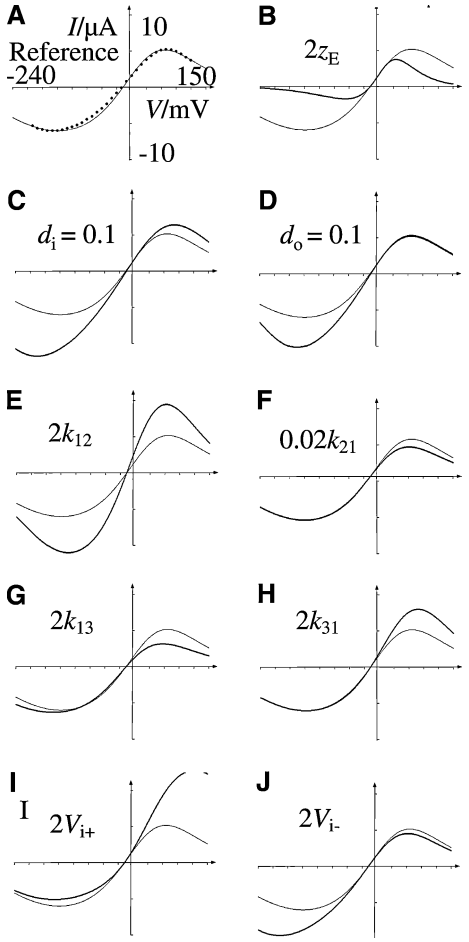


**Fig. 6.** Impact of individual parameters on model behavior. (*A*) Reference fit (Table 1, J; $V_c = +60$ m*V*, 50 mM $[K^+]_o$) with experimental data. (*B-J*) Same reference curve (*thin*) and deformation thereof (*bold*) due to change of individual parameter by marked factor.

Finally, doubling $V_{i+}$ and $V_{i-}$ results in a weaker inhibition of the transport function at positive and negative voltages, respectively (Fig. 6I, J), i.e., larger current amounts in the corresponding *V* range. This effect can be understood intuitively. In extreme cases ($V_{i+} \rightarrow \infty$, $V_{i-} \rightarrow -\infty$), there will be no inhibition at all within a finite *V* range, and the isolated transport function will appear as such (bold curve in Fig. 7) by elimination of the gating function ($f_i = 1$), which modulates the activity.

One may ask why the apparent *I-V* relationships, e.g., in Figure 4, are roughly symmetric but the amount of the positive voltage inhibition coefficient ($V_{i+}$) is much smaller than that of $V_{i-}$. Figure 7 provides the answer. The asymmetric *I-V* curve of the noninhibited open channel (bold line in Fig. 7) is steeper at moderately positive voltages than at moderately negative ones. This requires a stronger *V* inhibition in the positive range (small $V_{i+}$) for a roughly symmetric apparent *I-V* curve.

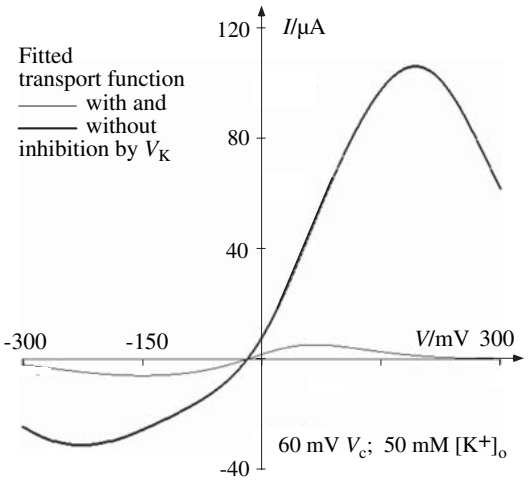


**Fig. 7.** Theoretical dissection of the mechanisms causing tilted-S *I-V*. *Thin curve*, fitted function from equation 1 with parameters listed in Table 1 (J) ($V_c = +60$ m*V*, 50 mM $[K^+]_o$), extrapolated to $\pm 300$ m*V*; *bold curve*, same function, except $f_i$ = const = 1, i.e., without inhibition by $V_K$.

## Interpretation

The numerical analysis of the experimental data presented here indicates that the characteristic tilted-S shape of the *I-V* relationship of Kcv is the result of two cooperating effects. First, there is the positive ratio $z_E/z_C$ (here 0.68/1.68, Table 1, J) between the apparent charge of the empty and the loaded binding sites in the transport function, which causes depletion of empty binding sites at large voltages of either sign. *Loaded* in this context means that all serial $K^+$ binding sites of the selectivity filter are occupied, and *empty* means that one of these sites is not occupied (*n* - 1). Interestingly, the finding $d_i$, $d_o \approx 0$ means electrodiffusion through the pore sections between the bulk solutions and the binding sites in the selectivity filter is much faster than the limiting enzymatic reaction cycle itself. These features, however, do not explain the intersection of the *I-V* relationships obtained at different $[K^+]_o$ (Fig. 5). These intersections rather point to a second effect of $K^+$, namely, an inhibition of the transport function by $V_K$. The analysis presented here points to a specific effect of the electrochemical $K^+$ driving force $V_K = V - E$; i.e., mere sensitivity to *V* or to $[K^+]$ cannot explain this behavior. This quantitatively verified specificity rules out many alternative inhibitory mechanisms, such as simple diffusion limitation or familiar voltage gating.

The present data and analysis do not resolve the temporal behavior of this inhibition. We assume that short periods of full activity (open state) alternate with short periods of $V_K$-induced inactivity (closed state). Thus, the autoinhibiting effect of $V_K$ investigated here corresponds to the known mechanism of fast *V*-dependent block by competing ions (Klieber & Gradmann, 1993).

Already qualitative inspection of the results in Figure 5 reveals that the voltages, $V_i$, of the characteristic, $\Delta[K+]_o$-induced intersections of the *I-V* relationships are shifted in parallel direction with $E_K$ when we compare the 20/50 mM $[K+]_o$ experiments (Fig. 5A and B, more negative $V_i$) with the 100/50 mM $[K+]_o$ experiments (Fig. 5C and D, more positive $V_i$). A mechanistic explanation for the inhibiting function $f_i(V_K)$ of $K^+$ worked out here and of $f_i(V_X)$ of nontransported cations X (fast voltage-dependent block) might be as follows. In the absence of a net driving force, the monomers of the selectivity filter are assumed to be elastically suspended by the P-loops in an optimal position for $K^+$ conductance. Both the electrical and the chemical components for ion movement to the filter exert a certain mechanical force on the mouth of the selectivity filter, when the substrate hits the rim of the orifice. This will result in a deformation of the channel mouth out of its optimal conductance conformation. In case of equal electrochemical forces from both sides, the effects will cancel each other and the selectivity filter will operate optimally. In other words, the familiar three-dimensional images of $K^+$ channels, in particular of the selectivity filter, should be viewed more as elastic structures than as rigid ones. This deformation mechanism differs from simple occlusion of the channel by nontransported ions because it applies not only to nontransported ions (familiar, voltage-dependent block) but also to the transported species (here $K^+$). Molecular dynamic simulations of the KcsA channel pore (Allen, Anderson & Roux, 2004) support this dynamic deformation mechanism. At present, such mechanistic interpretations are highly speculative however. The experimental evidence provided here refers to kinetic relationships only.

## Conclusions

Kinetic analysis of the open state *I-V* relationship of Kcv with different $V_c$ and $[K^+]_o$ yields the following qualitative features of the model in Figure 1:

1. The electrical distances $d_i$ and $d_o$ between the bulk solutions and the active center of the transporter are small. This means electrodiffusion through the access sections is fast compared to the turnover of the selectivity filter.
2. The apparent charge number $z_E$ of the empty ($n$ - 1) binding site is $\approx$0.6; $z_C$ of the fully $K^+$ loaded complex is $\approx$1.6.
3. The main effect of the conditioning voltage, $V_c$, on the reaction system can be assigned to an increase of p$K_a$ at more positive $V$ (and *vice versa*).
4. The electrochemical driving force for $K^+$, $V_K = V - E_K$ of either sign, autoinhibits the cord conductance of wt-Kcv in a similar way as fast $V$-dependent block by competing ions.

This work was supported by grants to A. M. (FIRB 2001 project RBAU01JT9C_001 from Ministero dell Università e della Ricerca MIUR).

## References

Allen, T.W., Anderson, O.S., Roux, B. 2004. On the importance of atomic fluctuations, protein flexibility, and solvent in ion permeation. *J. Gen. Physiol.* **124:**679–690

Blatt, M.R. 1986. Interpretation of steady-state current-voltage curves: Consequences and implications of current subtraction in transport studies. *J. Membr. Biol.* **92:**91–110

Doyle, D.A., Cabral, L.M., Pfuetzner, R.A., Kuo, A., Gulbis, J.M., Cohen, S.L., Chait, B.T., MacKinnon, R. 1998. The structure of the potassium channel: Molecular basis of $K^+$ conduction and selectivity. *Science* **280:**69–77

Fingerle, J., Gradmann, D. 1982. Electrical properties of the plasma membrane of microplasmodia of *Physarum polycephalum*. *J. Membr. Biol.* **68:**67–77

Gazzarrini, S., Van Etten, J.L., DiFrancesco, D., Thiel, G., Moroni, A. 2002. Voltage-dependence of virus-encoded miniature $K^+$ channel Kcv. *J. Membr. Biol.* **187:**15–25

Gradmann, D., Boyd, C.M. 2004. Current-voltage-time records of ion translocating enzymes. *Eur. Biophys. J.* **33:**396–411

Gradmann, D., Boyd, C.M. 2005. Apparent charge of binding site in ion translocating enzymes: Kinetic impact. *Eur. Biophys. J.* **34:**353–357

Hertel, B., Tayefeh, S., Mehmel, M., Kast, S.M., Van Etten, J., Moroni, A., Thiel, G. 2006. Elongation of outer transmembrane domain alters function of miniature K+ channel Kcv. *J. Membr. Biol.* 210:1–9

Klieber, H.G., Gradmann, D. 1993. Enzyme kinetics of the prime $K^+$ channel in the tonoplast of *Chara*: Selectivity and inhibition. *J. Membr. Biol.* **132:**253–265

Nichols, C.G., Lopatin, A.N. 1997. Inward rectifier potassium channels. *Annu. Rev. Physiol.* **59:**171–191

Pagliuca, C., Goetze, T.A., Wagner, R., Thiel, G., Moroni, A., Parcej, D. 2007. Molecular Properties of Kcv, a virus encoded $K^+$ channel. Biochemistry 46:1079–1090

Plugge, B., Gazzarrini, S., Nelson, M., Cerana, R., van Etten, J.L., Derst, C., DiFrancesco, D., Moroni, A., Thiel, G. 2000. A new potassium channel protein encoded by chlorella virus PBCV-1. *Science* **287:**1641–1644